Chapter 2

Dynamical Implications of Phosphorelay Circuit Structure

In this chapter, we ask how the bandpass and pulsatile features of the phosphorelay circuit affect the approach to sporulation in individual cells. We address this question through a combination of mathematical modeling and single-cell monitoring via time-lapse fluorescence microscopy. Our data show that the bandpass input functions of P_{0A} and P_{0F} are shifted relative to each other. A simple mathematical model incorporating these constraints (transcriptional bandpasses plus discrete pulses in kinase activity) predicts the additional post-translational bandpass regulation of Spo0A∼P activity by Spo0F expression level. The model also predicts the appearance of a delayed phase shift between pulses of P_{0A} and P_{0F} activity, after they have been in phase for several cell cycles. Our experiments verified the existence of this delayed phase shift. Further analysis of the model indicates the possibility of an additional state in which no phase shift appears between these promoter activity pulses. Consistent with this prediction, strains containing extra copies of *spo0F* showed additional steady-state-like behavior with no phase shift between P_{0A} and P_{0F} pulses. Together these results provide insight into the interplay between the periodic input to the sporulation circuit and the dynamics of its components.

2.1 Transcriptional Bandpasses

In order to characterize the feedback dynamics of the sporulation circuit, we first investigated the quantitative dependence of the activity of the *spo0A* and *spo0F* promoters, denoted P_{0A} and P_{0F}, respectively, on Spo0A∼P levels. To do so, we took advantage of

the Spo0A^{sad67} allele, which is known to transcriptionally regulate target promoters without the need for phosphorylation [23, 31]. We constructed two strains (Fig. 2.1a) in which Spo0A^{sad67} controlled expression of the yellow fluorescent protein, YFP, from either the P_{0A} or the P_{0F} promoter. In both strains, Spo0A^{sad67} was expressed from the IPTG-dependent $P_{hyperspank}$ inducible promoter, denoted P_{hyp} [23]. These strains also incorporated a second copy of P_{hyp} driving expression of cyan fluorescent protein, CFP, for calibration.

At the start of the experiment, each of the two strains was induced with the same amount of IPTG, and imaged over time using time-lapse microscopy (Fig. 2.1b). As Spo0A^{sad67} expression levels increased towards their steady state value, we quantified the activity of the downstream promoters, determined by the rate of increase in YFP fluorescence (see Appendix B), as well as the mean fluorescence of the calibration reporter (Fig. 2.2a,b) [17, 19, 37, 58, 59]. Then, we plotted these P_{0A} and P_{0F} promoter activities against the level of the calibration reporter (and thus of Spo0A^{sad67}) from the same cell (Fig. 2.2c,d). For both promoter reporters, these measurements were performed on cells growing in similar microenvironments and fluorescent illumination conditions.

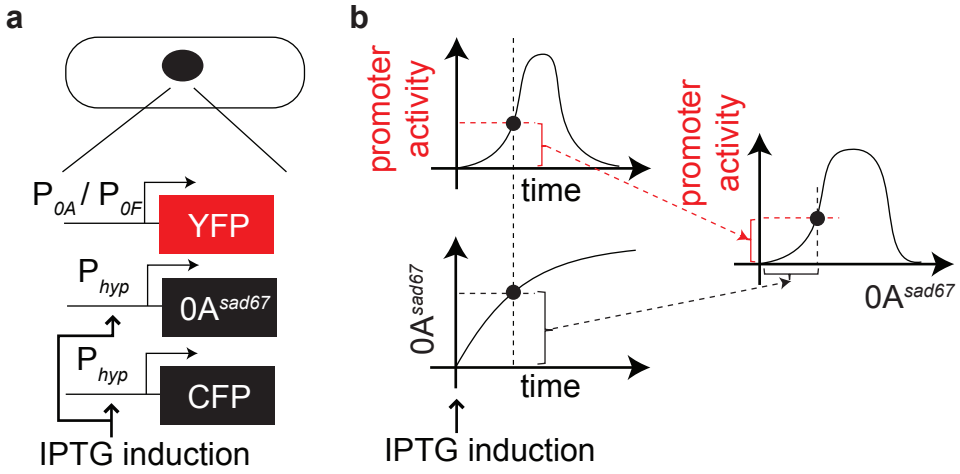

Figure 2.1: (a) Schematic of the strains and (b) the method used to measure the bandpass functions of P_{0A} and P_{0F}.

The data provided a quantitative measurement of the bandpass input functions for P_{0A} and P_{0F} (Fig. 2.2c,d and Fig. 2.3). Despite variability, we found that the two promoter reporters displayed both broadly similar features and systematic differences. Thus, although they exhibited coincident pulses of activity, P_{0A} exhibited greater basal fluorescence ex-

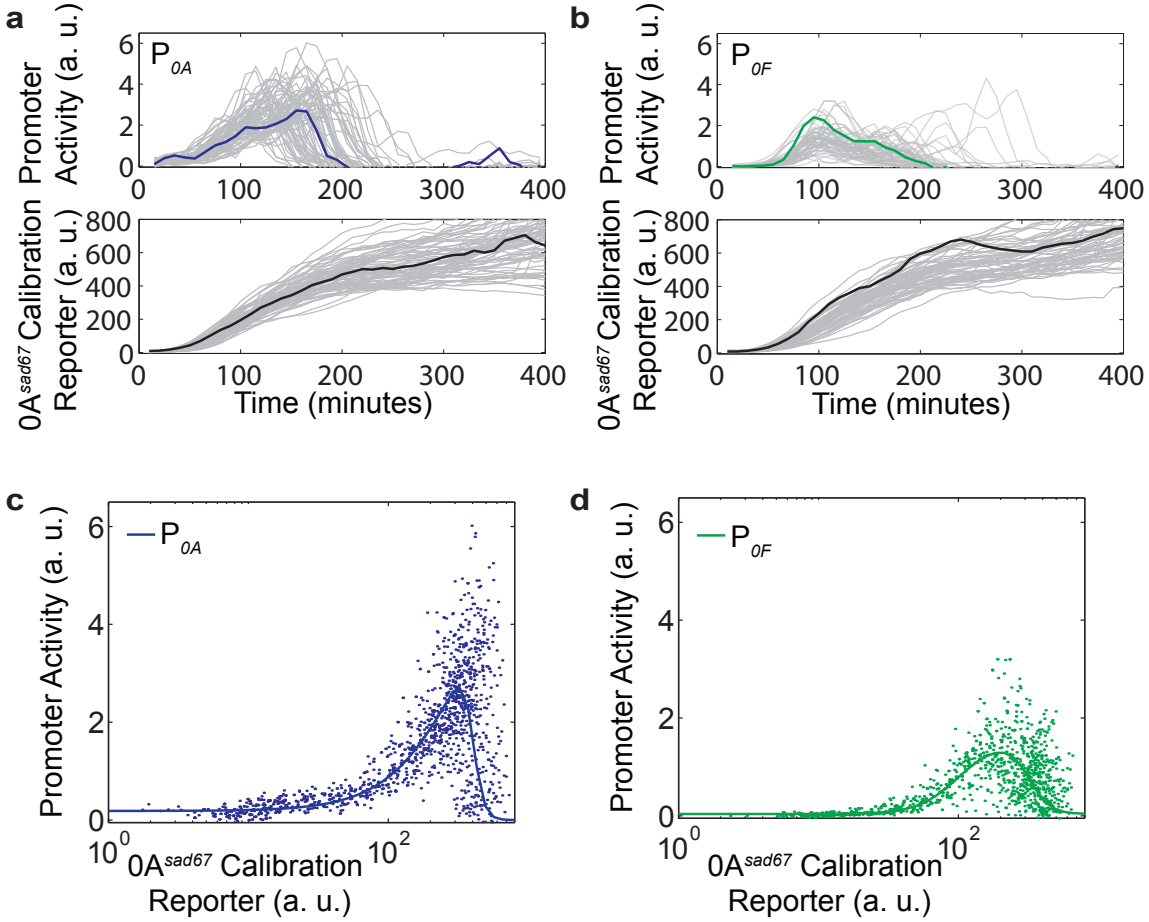

Figure 2.2: Transcriptional bandpasses in the sporulation initiation circuit. (a)–(b) Single-cell measurements of promoter activities of P_{0A} ($N = 75$) and P_{0F} ($N = 64$) (top panels), and corresponding induction profiles of the Spo0A^{sad67} calibration reporter (bottom panels). Individual traces are shown in gray. A specific trace in each plot is highlighted in color line. (c)–(d) Single-cell measurements represented as P_{0A} /P_{0F} promoter activity versus the Spo0A^{sad67} calibration reporter (dots). Solid lines show a fit resulting from the following set of parameter values: $n_A = 1.6$, $m_A = 12$, $n_F = 3$, $m_F = 6$, $K_F = 100 a.u.$, $K_A = 3.5K_F$, $J_A = 4K_F$, $J_F = 3.2K_F$, $\alpha_{0A} = .4K_F$, $\alpha_{0F} = 0.025$, $\beta_{0A} = 6 a.u.$, $\beta_{0F} = 1.5 a.u.$.

pression at low Spo0A^{sad67} levels, a higher total fluorescence expression level, and a sharper shutoff at high Spo0A^{sad67} levels, compared to P_{0F}.

To gain insight into the origins of the observed variability, we compared the difference between a cell and its sister cell with the difference between the same cell and a randomly chosen surrogate sister cell (Appendix Fig. B.1). Here, the difference metric for two given traces is the cumulative sum in time of the absolute difference between them. The difference between sister cells was significantly smaller than that between surrogate sister cells (Appendix Fig. B.1), suggesting that variable features can be inherited between cell generations.

In order to incorporate the measured bandpass functions into a model of the phosphorelay circuit, we modeled the experimental data using standard promoter activity rate functions that incorporate both activation and repression (solid lines, Fig. 2.2c,d):

$$P_{0A} = \beta_{0A} \frac{\alpha_{0A}^{n_A} + x^{n_A}}{K_A^{n_A} + x^{n_A}} \frac{J_A^{m_A}}{J_A^{m_A} + x^{m_A}}, \tag{2.1}$$

$$P_{0A} = \beta_{0F} \left(\alpha_{0F} + \frac{x^{n_F}}{K_F^{n_F} + x^{n_F}} \frac{J_F^{m_F}}{J_F^{m_F} + x^{m_F}} \right). \tag{2.2}$$

Here, x represents [Spo0A$\sim$P], while the K_i and J_i parameters represent, respectively, the activation and repression thresholds of the transcriptional bandpasses. A heuristic fit of this model to the data is shown in Fig. 2.2c,d and in Fig. 2.3.

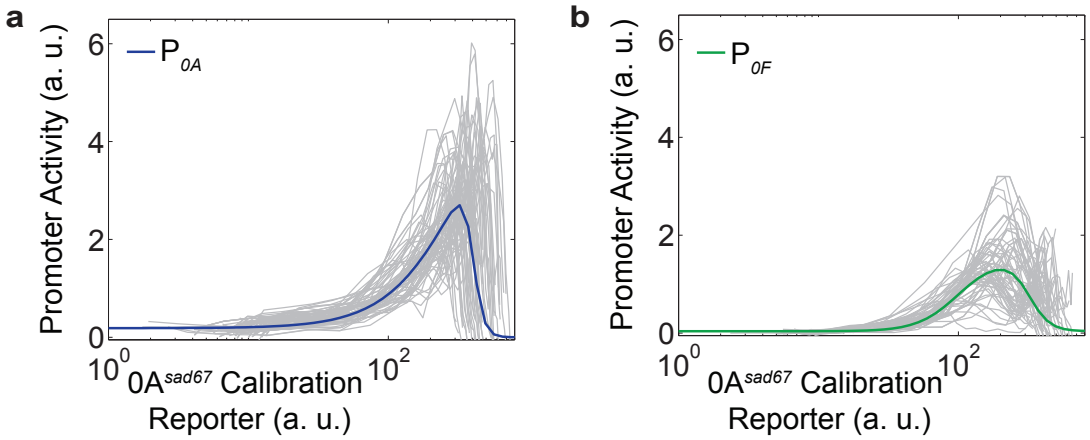

Figure 2.3: Transcriptional bandpasses in the sporulation initiation circuit. (a)–(b) Single-cell measurements represented as P_{0A} /P_{0F} promoter activity versus the Spo0A^{sad67} calibration reporter. Individual traces are shown in gray. Green and blue lines are the heuristic fits from Fig. 2.2c,d.

Together, these results show that P_{0A} and P_{0F} encode similarly shaped bandpass functions, but with systematic differences in their quantitative parameters.

2.2 Post-Translational Bandpass

Next, we constructed a simple mathematical model of the phosphorelay based on its phosphorylation, dephosphorylation, and phosphotransfer reactions. These reactions are modeled using ordinary differential equations based on standard mass action kinetics. The model consists of four equations representing the phosphorylated forms of the phosphorelay proteins KinA (K_p), Spo0F (F_p), Spo0B (B_p), and Spo0A (A_p),

$$\begin{aligned}
\frac{dK_p}{dt} &= k_s(K_T - K_p) - k_t K_p(F_T - F_p), \\
\frac{dF_p}{dt} &= k_t K_p(F_T - F_p) - k_t F_p(B_T - B_p) + k_{-t} B_p(F_T - F_p) - k_h(K_T - K_p)F_p - k_r F_p, \\
\frac{dB_p}{dt} &= k_t F_p(B_T - B_p) - k_{-t} B_p(F_T - F_p) - k_t B_p(A_T - A_p) + k_{-t} A_p(B_T - B_p), \\
\frac{dA_p}{dt} &= k_t B_p(A_T - A_p) - k_{-t} A_p(B_T - B_p) - k_e A_p.
\end{aligned}$$

Here, K_T, F_T, B_T, and A_T represent total levels of the phosphorelay proteins, $k_{\pm t}$ is the rate of forward/backward phosphotransfer rates in the phosphorelay, k_s is the rate of autophosphorylation of the kinase, k_e and k_r are the dephosphorylation rates of Spo0A and Spo0F by their phosphatases, respectively, and k_h is the rate of dephosphorylation of Spo0F by KinA. The parameter values used for this set of equations are listed in Table 2.1. The choice of these parameter values was guided by the notion that reactions mediating phosphate flux are typically faster than the cell-cycle timescale ($\sim 1/hr$). The rate constants for the bimolecular reactions in the model (see Table 2.1) are similar to effective rate constants for the phosphotransfer reactions estimated from *in vitro* experiments [28].

Using this model, we first computed the response of A_p to different Spo0F expression levels and observed a bandpass response (Fig. 2.4). Removal of reverse phosphotransfer from the model ($k_{-t} = 0$) completely abolishes the inhibition of A_p by high Spo0F levels (Appendix Fig. C.1a,c), showing that reverse phosphotransfer is necessary for this bandpass response. Similarly, when the Spo0F phosphatase activity is set to zero in the model ($k_r = k_h = 0$), high levels of Spo0F do not inhibit A_p (Appendix Fig. C.1b,c). This bandpass response is also seen in a more realistic model of the phosphorelay circuit that

Parameter	Value
K_T	$1000nM$
B_T	$1000nM$
A_T	$1000nM$
$k_{\pm t}$	$1/(nM \cdot hr)$
k_s	$100/hr$
k_r	$100/hr$
k_e	$100/hr$
k_h	$1/(nM \cdot hr)$

Table 2.1: Parameters for the phosphorylation, phosphotransfer, and dephosphorylation reactions of the phosphorelay circuit model.

includes cell-cycle-dependent pulsing and transcriptional feedbacks (Appendix Fig. C.2a–c), as well as in a more complicated reaction scheme of the core phosphorelay (Appendix C, Appendix Fig. C.2d). Thus, the bandpass response of Spo0A phosphorylation to Spo0F levels in this model is a direct result of reversibility of the phosphotransfer, which allows phosphates to flow backwards from Spo0A to Spo0F, where they can be hydrolyzed by Spo0F phosphatases and lost from the system.

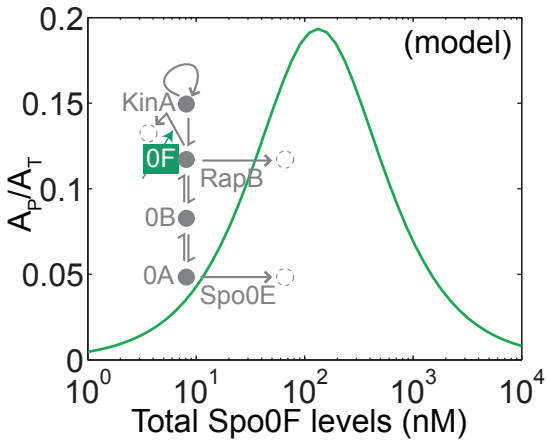

Figure 2.4: Phosphorelay activity depends on total Spo0F levels in a bandpass manner. Fraction of phosphorylated Spo0A computed for different Spo0F levels in the phosphorelay model.

Experiments confirm the post-translational bandpass of phosphorelay activity. The prediction that Spo0F levels have a bandpass effect on Spo0A activity is in qualitative agreement with previous experimental results [13]. To measure the post-translational bandpass at the level of single cells, we induced Spo0F to different levels using a Spo0F-CFP protein under the IPTG-controlled promoter P_{hyp} in a strain where the endogenous

copy of *spo0F* was deleted (Fig. 2.5). We quantified the resulting activity of Spo0A∼P activity by measuring the peak amplitude of the P_{0F}-YFP pulses. We observed a striking bandpass response similar to that predicted by the model (Fig. 2.6). The physiological response of sporulation was inhibited at the highest IPTG induction (results not shown), indicating that the bandpass response is due to low Spo0A∼P and not an artifact of the transcriptional bandpass in the P_{0F} reporter.

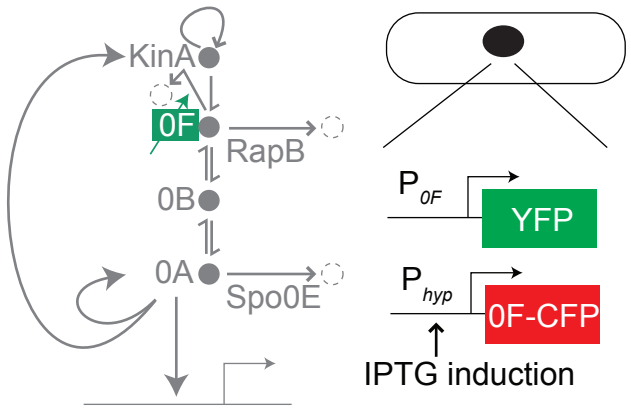

Figure 2.5: Diagram of the sporulation circuit and the strain schematic used to test the post-translational bandpass prediction (compare to Fig. 1.2).

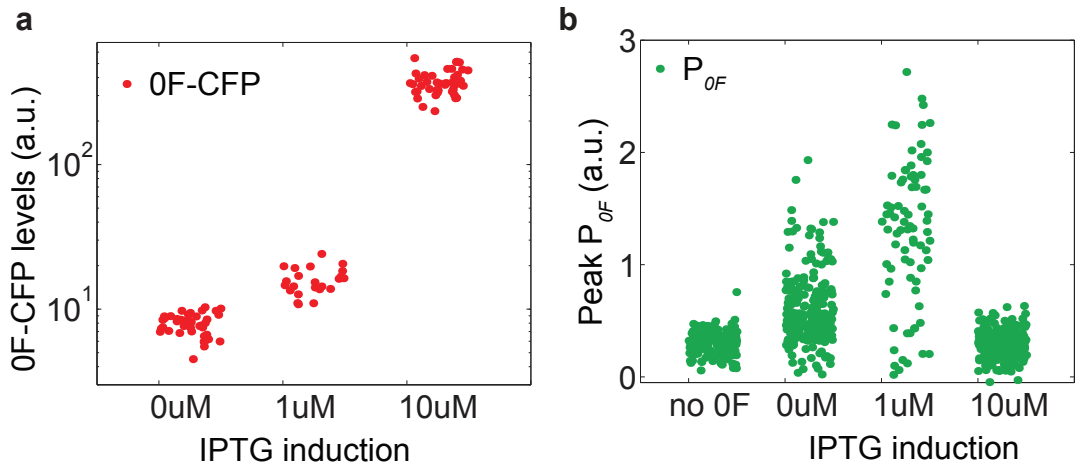

Figure 2.6: Measurement of the Spo0F post-translational bandpass. (a) As the amount of inducer IPTG is increased (0uM, 1uM, 10uM), there is an increase in Spo0F induction level. (b) Peak P_{0F} pulse amplitude over time for different IPTG induction levels has a bandpass shape. There is some activity even at 0uM IPTG possibly due to basal expression of Spo0F, although it is too low to induce sporulation.

2.3 Delayed Phase Shift

Next, we incorporated the cell-cycle-dependent pulsatile regulation of phosphorelay activity into the model. For simplicity, we assumed that the kinase autophosphorylation rate is a square wave ($k_s(ON/OFF)$), with a period fixed at 3 hours, similar to the cell-cycle times observed experimentally (Fig. 2.7). We further assumed, arbitrarily, that the duration of the "ON" phase spanned 50% of that period. We also included in the model the feedbacks on the phosphorelay proteins based on the transcriptional bandpass measurements. In this more complete model, the total level of each phosphorelay protein can increase due to transcription and decrease by degradation. While both phosphoforms can be degraded, we assume that transcription creates only unphosphorylated proteins. These reactions are also modeled using ordinary differential equations. Because there are no known active degradation processes for these proteins, we assume that the only source of degradation is dilution by cell growth, which is modeled as a first-order decay process with rate constant γ. With these assumptions, we obtain the following equations for the total concentrations of the phosphorelay proteins KinA, Spo0F, Spo0B, and Spo0A, denoted K_T, F_T, B_T, and A_T, respectively:

$$\begin{aligned}
\frac{dK_T}{dt} &= P_{kinA}(A_p) - \gamma K_T, \\
\frac{dF_T}{dt} &= P_{0F}(A_p) - \gamma F_T, \\
\frac{dB_T}{dt} &= P_{0B} - \gamma B_T, \\
\frac{dA_T}{dt} &= P_{0A}(A_p) - \gamma A_T.
\end{aligned}$$

Here we assume that protein degradation is negligible compared to protein dilution. Hence, $\gamma = 1/hr$, similar to the rates of dilution by cell growth observed experimentally. This degradation term is also added to the equations of the phosphorylated proteins. The mean rates of expression from the P_{0F} and P_{0A} promoters, as functions of Spo0A$\sim$P(A_p), are denoted $P_{0F}(A_p)$ and $P_{0A}(A_p)$, respectively, and are based on the empirically determined bandpass functions, given by Eqs.(2.1)–(2.2). The bandpass parameters are constrained by the experimental measurements above, with the free parameter K_F chosen to be $K_F = 100nM$, similar to values of Spo0A$\sim$P's DNA binding affinity estimated from previous experiments [22]. Additionally, because previous results suggest that the promoter of KinA is also a band-

pass like that of Spo0A [24], we assume that $P_{kinA}(A_p) = P_{0A}(A_p)$ (the importance of this assumption is checked in the dynamical analysis described below). There is no known transcriptional regulation of Spo0B by Spo0A∼P. Moreover, experimental measurements show that expression level of a fluorescent reporter fused to P_{0B} is already turned on prior to the beginning of progression to sporulation, and that this reporter changes less than twofold during sporulation initiation (Appendix Fig. B.2). Consequently, we assume P_{0B} to be constant, $P_{0B} = \beta_{0B}$. The maximal expression strengths of these promoters are free parameters and are set to $\beta_{0A} = 15000nM/hr$, $\beta_{0B} = 6000nM/hr$, $\beta_{0F} = 2280nM/hr$. The parameters used in this set of equations are summarized in Table 2.2.

Parameter	Value
$k_s(ON)$	$100/hr$
$k_s(OFF)$	$1/hr$
γ	$1/hr$
n_A	1.6
m_A	12
n_F	3
m_F	6
K_F	$100nM$
K_A	$3.5K_F$
J_A	$4K_F$
J_F	$3.2K_F$
α_{0A}	$0.4K_F$
α_{0F}	0.025
β_{0A}	$15000nM/hr$
β_{0F}	$2280nM/hr$
β_{0B}	$6000nM/hr$

Table 2.2: Parameters for the periodic input and the production-degradation reactions of the phosphorelay circuit.

In order to understand the implications of the bandpass regulation on the dynamics of the phosphorelay in cells, we first set out to simplify the model by reducing its dimensionality. The model has eight dimensions: expression levels of the four proteins and their phosphorylation states. However, because the timescale of phosphorylation is much faster than that of protein production and degradation, the four degrees of freedom corresponding to phosphorylation can be adiabatically eliminated. In addition, since P_{0B} is constant, B_T can be set to a fixed value. Third, having assumed $P_{kinA} = P_{0A}$, KinA and Spo0A protein levels are represented by the same degree of freedom. These considerations allow

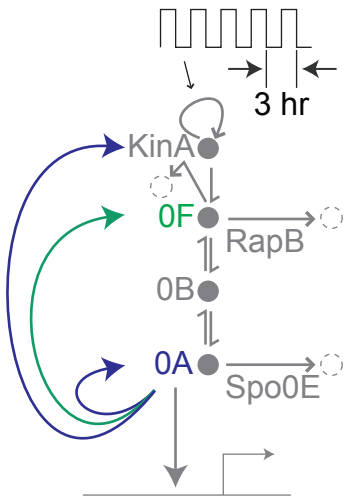

Figure 2.7: Diagram of the phosphorelay circuit driven by square wave pulses in kinase autophosphorylation.

us to reduce the model to two effective dimensions, one for total Spo0A and another one for Spo0F:

$$\begin{aligned} \frac{dF_T}{dt} &= P_{0F}(A_p) - \gamma F_T, \\ \frac{dA_T}{dt} &= P_{0A}(A_p) - \gamma A_T. \end{aligned}$$

In this reduced model, the promoter activities P_{0A} and P_{0F} are functions of A_p, which itself is a function of the values of the total levels of the phosphorelay proteins and the input square wave. This dependence is computed from the equations of the phosphorylated proteins (see Appendix C).

To analyze the dynamic behavior of this two-dimensional model, we computed the nullclines $\frac{dF_T}{dt} = 0$ and $\frac{dA_T}{dt} = 0$ on the Spo0A-Spo0F phase plane. The trajectories in the two-dimensional model switch between two phase planes, corresponding to the "ON" and "OFF" parts of the square wave (Fig. 2.8). For the parameters chosen, the nullclines cross at a single point in both phase planes, which is a stable steady state. Consider the trajectory starting near the origin, where levels of phosphorelay proteins are low (gray and red lines in Fig. 2.8). Such a trajectory spends the first few periods traversing up and down a single line passing through the origin, for which Spo0A and Spo0F are proportional to (i.e., in phase with) each other, and then curves away from this line (see Fig. 2.8). At that point

the proportionality between Spo0A and Spo0F breaks down, leading to the appearance of a phase shift between the activities of the P_{0A} and P_{0F} promoters (Fig. 2.9). The assumption that $P_{kinA}(A_p) = P_{0A}(A_p)$ does not qualitatively change the dynamical picture described here (Appendix Fig. C.3).

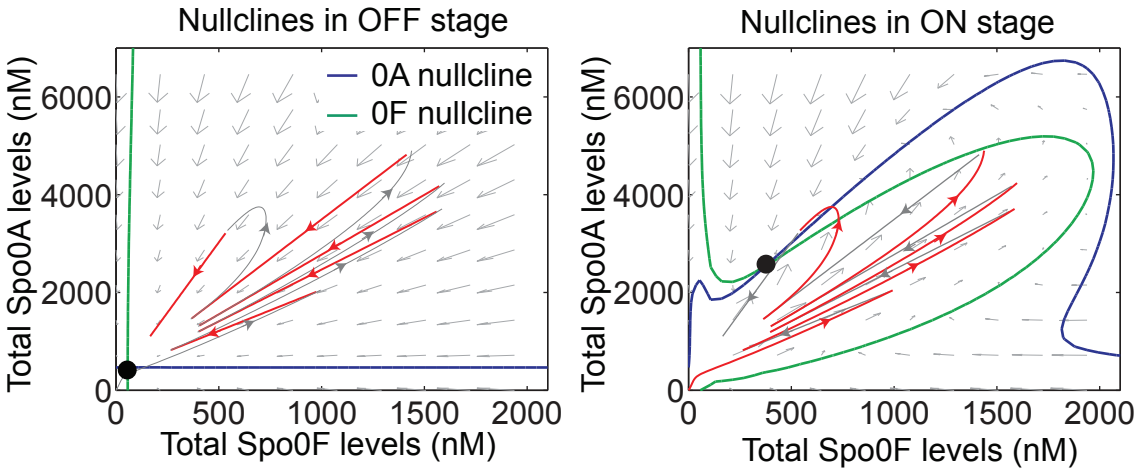

Figure 2.8: Phase portraits computed from the reduced model for "ON" and "OFF" parts of the square wave: Solid lines represent nullclines of Spo0A (blue) and Spo0F (green), arrows depict the slope field, and black circles denote stable steady states. A red-gray color code is used to plot the trajectory on each phase plane, with red marking the portion of the trajectory that evolves on the active phase plane, and gray marking the portion on the other phase plane.

The emergence of this delayed phase shift from the model can be understood in terms of the effect on the transcriptional bandpass functions of P_{0A} and P_{0F} (Fig. 2.10). In the initial periods of the square wave, the peak amplitude of Spo0A∼P pulse is low and it accesses only the activating parts of the promoter input functions. Consequently, the pulses in P_{0A} and P_{0F} are proportional to each other. In the last period, the peak amplitude of Spo0A∼P is higher and it sweeps across the bandpass region. When this happens, there is a time interval in which P_{0F} is repressed while P_{0A} is activated, generating a phase shift between the P_{0A} and P_{0F} pulses. The duration of this phase shift is determined by the rate of increase in Spo0A∼P level, with a faster rate of increase resulting in a smaller duration. In the limit that Spo0A∼P levels reach their final value instantaneously, there is no phase shift.

Delayed phase shift between P_{0A} and P_{0F} can be observed experimentally. To verify experimentally the existence of this delayed phase shift between the activities of

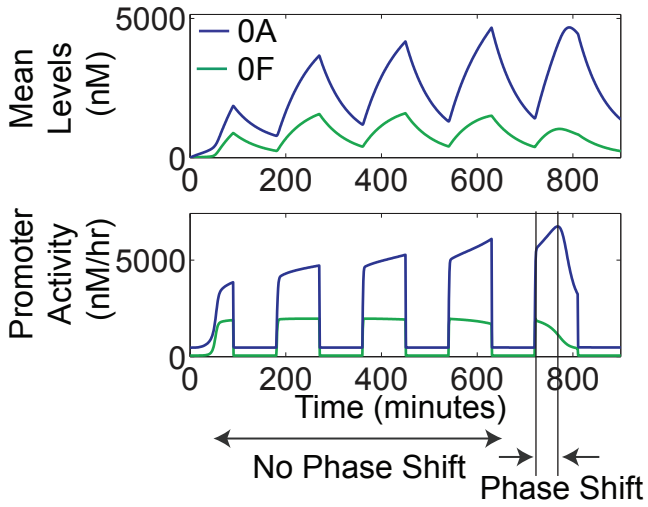

Figure 2.9: Delayed phase shift emerges in the periodic activity of genes P_{0A} and P_{0F} in the phosphorelay circuit. Mean levels of Spo0A and Spo0F (top panel) computed from the complete model, and their corresponding promoter activities (bottom panel).

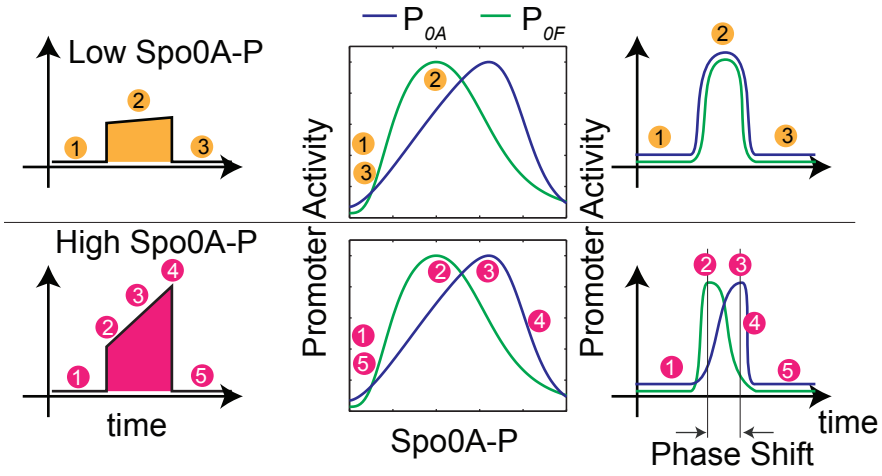

Figure 2.10: Illustration of the delayed phase shift as a mapping from a Spo0A∼P pulse to the transcriptional bandpasses, and from these bandpasses to the promoter activity pulses. Orange circles (top row, 1-2-3) label time-points before, during, and after a low amplitude Spo0A∼P pulse. Pink circles (bottom row, 1-2-3-4-5) label time-points before, during, and after a high amplitude Spo0A∼P pulse. Colored circles are placed at corresponding points on the transcriptional bandpasses and promoter activity pulses.

P_{0A} and P_{0F}, we constructed a two-color strain by which the two promoter activities could be simultaneously measured in the same cell (Fig. 2.11a). Both P_{0A} and P_{0F} pulsed in the sporulation cycles as well as in the pre-sporulation growth cycles (Fig. 2.11b). We found that the distribution of delays between P_{0A} and P_{0F} pulse peaks in the pre-sporulation growth cycles (Fig. 2.11c) is close to zero (1 ± 16 min, $N = 56$), i.e., the promoters pulse in phase, while those in the sporulation cycle are significantly larger than 0 (29 ± 26 min, $N = 83$; KS test, $p < 10^{-7}$).

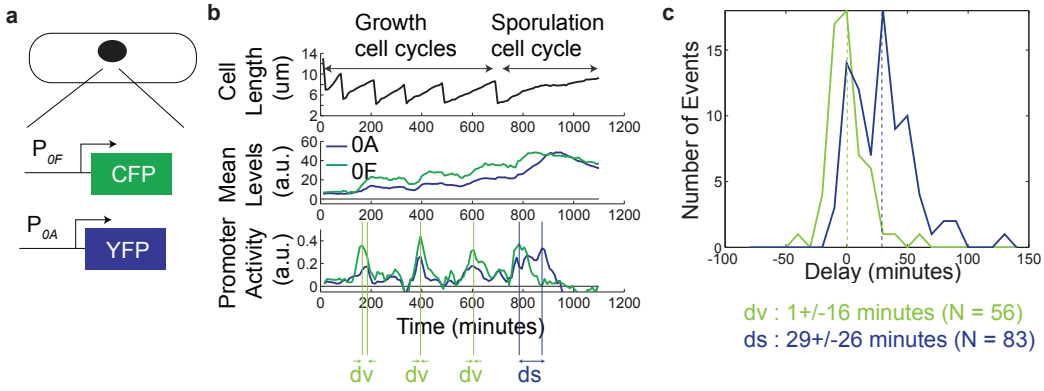

Figure 2.11: Delayed phase shift between P_{0A} and P_{0F} can be observed experimentally. (a) Schematic of the two-color strain used to experimentally measure the single-cell dynamics of P_{0A} and P_{0F}, which are fused to YFP and CFP fluorescent reporters, respectively. (b) Single-cell measurements of P_{0A} and P_{0F} promoter activities (bottom panel), mean levels of YFP and CFP (middle panel), and the cell length (top panel). "dv" and "ds" denote the time difference between the P_{0A} and P_{0F} peak pulse amplitudes in the pre-sporulation vegetative growth cycles and in the sporulation cycle, respectively. (c) Experimentally measured distribution of the P_{0A}-P_{0F} time differences in pre-sporulation vegetative growth cycles and in sporulation cycles.

2.4 Alternate Cellular State

Nullcline analysis of the simplified two-dimensional model is also useful in connecting the delayed phase shift in the phosphorelay dynamics with the post-translational bandpass (Fig. 2.4). In the "ON" phase plane, an increase in *spo0F* copy number (Fig. 2.12) shifts the Spo0F nullcline to the right, which leads to a low A_p fixed point (Fig. 2.13). In this situation, pulses of KinA activity lead to trajectories in phase space for which Spo0A and Spo0F are proportional for the duration of the square wave input. The promoter activities P_{0A} and P_{0F} also maintain their proportionality, and so exhibit no phase shift (Fig. 2.14).

Thus, the model predicts that an increase in *spo0F* copy number should lead to an alternate behavior with low levels of Spo0A∼P, where P_{0A} and P_{0F} pulse permanently in phase with each other.

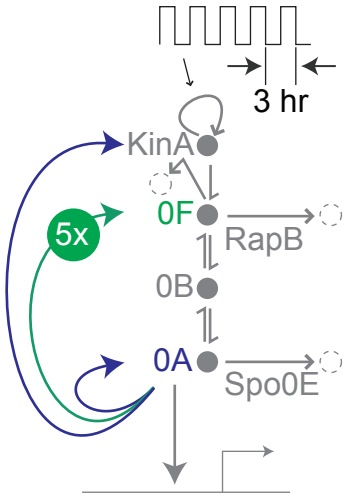

Figure 2.12: Diagram of the phosphorelay circuit with increased *spo0F* copy number.

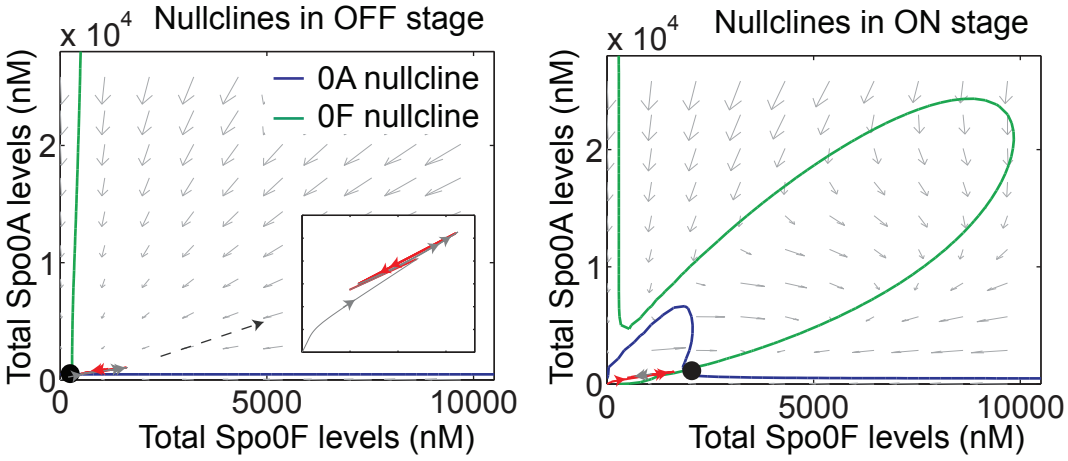

Figure 2.13: Phase portraits computed from the reduced model with increased *spo0F* copy number for the "ON" and "OFF" parts of the square wave.

In terms of the representation in Fig. 2.10, this perturbation in *spo0F* copy number restricts Spo0A∼P activity to low amplitude pulses. Since low amplitude Spo0A∼P pulses can give rise to pulses in P_{0A} and P_{0F}, this perturbed trajectory is similar to the initial periods of the square wave where P_{0A} and P_{0F} pulses are in phase (Fig. 2.9). However, these initial periods are limited in number, whereas in the perturbed system, the phase shift

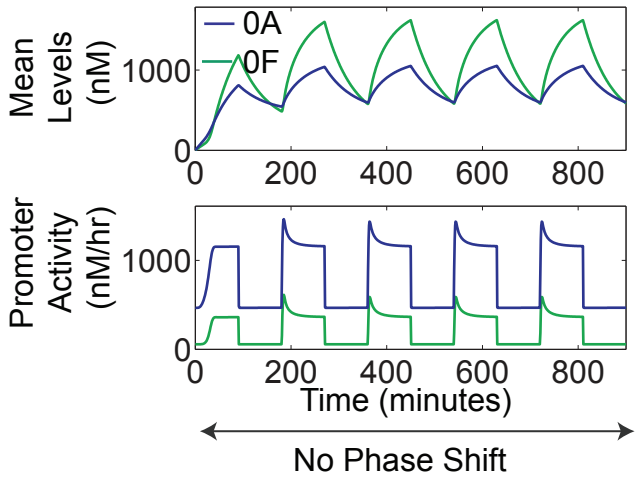

Figure 2.14: No phase shift in perturbed model. Mean levels of Spo0A and Spo0F (top panel) computed from the complete model, and their corresponding promoter activities P_{0A} and P_{0F} (bottom panel).

never appears (Fig. 2.14).

To investigate the dependence of the alternate state on the two types of bandpasses in the model, we examined the changes to the nullclines in response to individual bandpass perturbations. In the absence of reverse phosphotransfer, a feature needed for the post-translational bandpass, there is no alternate state, but the nullclines are strongly perturbed and change their orientation (Appendix Fig. C.4a,b). When the activation and repression parts of the P_{0F} transcriptional bandpass are removed individually, the nullclines are perturbed so that the alternate state exists (Appendix Fig. C.4a,c,d). In comparison to this, when the activation and repression parts of the P_{0A} transcriptional bandpass are removed individually, the nullclines are perturbed but without the appearance of the alternate state (Appendix Fig. C.4a,e,f). So, to a first approximation, it is the coupling of the post-translational bandpass and the P_{0F} transcriptional bandpass that enables the alternate state. Further analysis will be required to map regions in parameter space where the alternate state behavior exists.

To test the predicted effects of increased *spo0F* copy number, we first cloned the entire *spo0F* gene into pHP13, a plasmid with copy number ~ 5 [58]. We transformed this plasmid into the two-color P_{0A}-P_{0F} reporter strain (Fig. 2.15a), and used it to measure the phase shift between P_{0A} and P_{0F}. The distribution of delays between P_{0A} and P_{0F} pulse peaks (-7 ± 13 minutes, $N = 48$) indicates that their activities are in phase, consistent with the

model (Fig. 2.15c,d). Moreover, an additional, indirect line of evidence suggests that cells are in a state resembling the low Spo0A∼P alternate state. The level of Spo0A∼P in these cells is not high enough to initiate sporulation (Fig. 2.15b), but is high enough to elicit pulses in P_{0A} and P_{0F} promoter activities (Fig. 2.15d). Thus Spo0A∼P levels are low, but non-zero. Together, these experimental data qualitatively support the model prediction of an alternate state with higher Spo0F copy number.

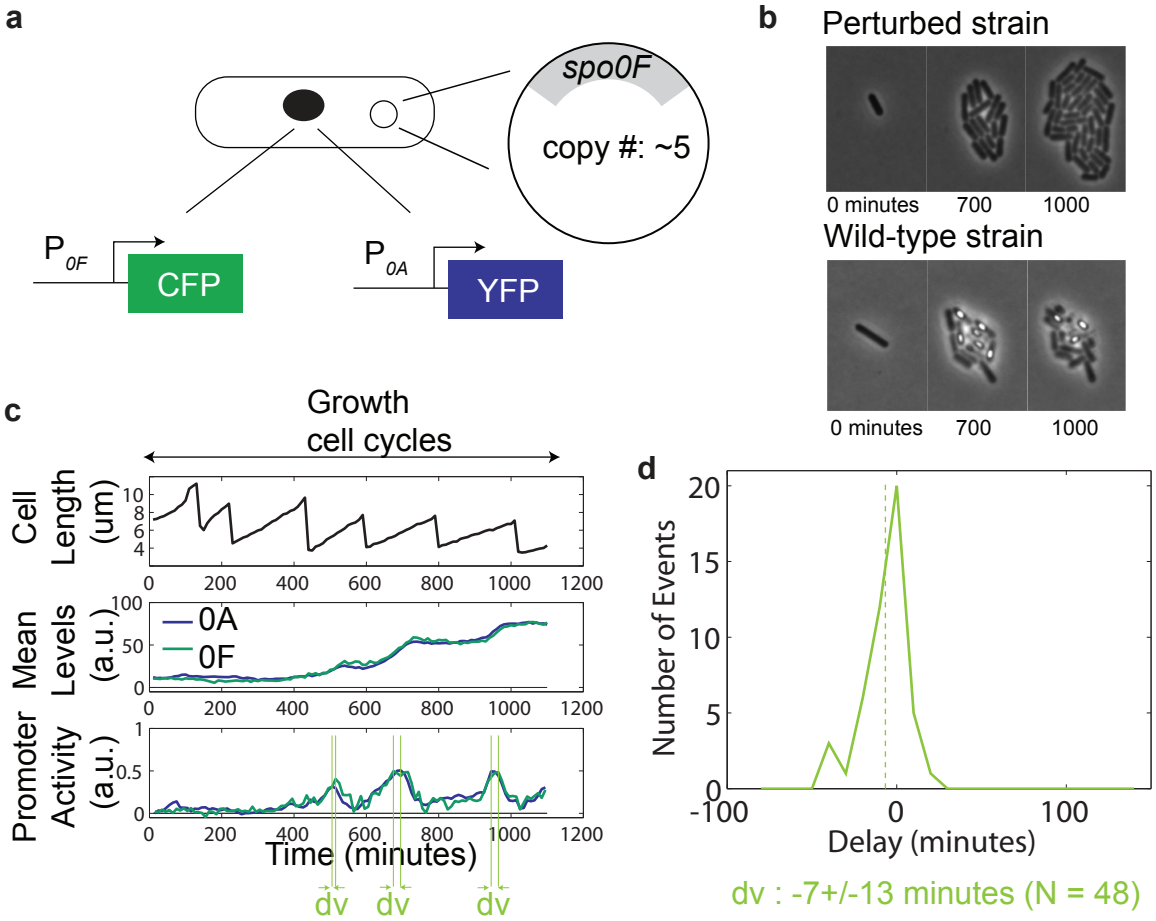

Figure 2.15: Increase in Spo0F copy number leads to a non-sporulating alternate state in which there is no phase shift. (a) Schematic of the strain used to experimentally test the alternate state prediction. (b) Frames from time-lapse movies showing that sporulation in the perturbed strain is inhibited in comparison to the wild-type strain. (c) Single-cell measurements of P_{0A} and P_{0F} promoter activities (bottom panel), mean levels of YFP and CFP (middle panel) and the cell length (top panel). "dv" denotes the time difference between the P_{0A} and P_{0F} peak pulse amplitudes in the pre-sporulation vegetative growth cycles. (d) Experimentally measured distribution of the P_{0A}-P_{0F} time differences in pre-sporulation vegetative growth cycles.

2.5 Interplay between Periodic Input and Circuit Dynamics

The central element of the sporulation circuit in *B. subtilis* is a phosphorelay embedded in bandpass transcriptional feedback loops, which are activated in a pulse-like manner, once per cell cycle. We have investigated the dynamical consequences of this particular architecture through a combination of single-cell monitoring and mathematical modeling. Our mathematical model reveals several striking features of this system, all of which are confirmed experimentally at the single-cell level: First, the response of Spo0A∼P activity has a bandpass dependence on Spo0F protein concentration. Second, pulses in the Spo0A and Spo0F promoter activities are in phase within the initial cell cycles subsequent to stress, but eventually develop a phase shift. Third, an alternate cellular state can be accessed, in which P_{0A} and P_{0F} pulse and remain in phase indefinitely, signifying the presence of low amplitude Spo0A∼P pulses. Together, these results show how pulsing together with bandpass-like features in a feedback circuit gives rise to surprisingly complex dynamics in the lead-up to sporulation.

According to our model, the emergence of the delayed phase shift depends on the interrelationship between the periodic input to the sporulation circuit and the dynamics of the circuit components. In particular, the phase shift appears when the Spo0A∼P pulse amplitude is high enough to access the repressing part of the transcriptional bandpasses. Thus, the rate of increase of Spo0A∼P determines the number of periods needed for the phase shift to appear. Additionally, in a given period, the magnitude of this rate in comparison to the relative duration of the "ON" phase plays a role in determining the maximal value of Spo0A∼P pulse. If the rate is too slow, then Spo0A∼P pulse is shut off before it reaches a value large enough to generate a phase shift, as seen in the earlier periods. Only if the rate is high enough, does the Spo0A∼P pulse rise to a value large enough to generate a phase shift before it is turned off. These are important considerations as the rate of increase of Spo0A∼P determines the duration of the phase shift, and consequently the timing of the sequence of events leading to the transition to sporulation.

An inherent challenge in the model is to map the relationship between perturbations in the transcriptional bandpasses and the sporulation dynamics. Currently, this is hindered by a limited understanding of how Spo0A∼P interacts with the promoter regions of P_{0A} and P_{0F} to generate the bandpass mode of regulation. An approach that determines how

bandpass regulation is encoded in the promoter architectures will be required to overcome this. This will also be useful in corroborating the parameter estimates reported here or in obtaining more exact ones. In particular, while this study shows that the P_{0A} and P_{0F} transcriptional bandpasses are quantitatively different, further studies may be required to determine the exact ratios of the bandpass thresholds and their slopes. More generally, while the parameters for production-degradation and phosphorylation-dephosphorylation-phosphotransfer used here are reasonable, determining their exact values may require further investigation. Following this, the model can be combined with systematic perturbations to the promoters to develop further insight into the dynamics leading to sporulation initiation.

Studies of terminal differentiation dynamics in individual cells can reveal the fine structure behavior of underlying regulatory circuits. Here, this behavior takes the form of the emergence of a delayed phase shift and the capability, in an alternate state, to suspend the appearance of the phase shift. Fine-structure studies of other circuits regulating terminal differentiation may reveal further instances of temporal order in gene expression. Dynamic single-cell studies of other processes should reveal if constituent genes are sequentially expressed, and if this temporal order is operationally critical or is just a by-product of resource optimization by cells preparing for a terminal state [68].